Determination of the Earthquake Source Parameters in the Aswan Area, Egypt

M. Salem[2], E. M. El-Amin[1], H. Zahra[2], I .Abu El Nader[1], and H. Lofty[1]

[1]National Research Institute of Astronomy and Geophysics
[2]Geology Department, Faculty of Science, Benha University
E-mail: mohamed.salem@fsc.bu.edu.eg

Abstract

The Aswan region is seismically active, according to Egypt's seismotectonic studies. This region served as the epicenter of the November 14, 1981, ML, 5.5 earthquake that seriously destroyed Aswan and the neighborhood. The source parameters of Aswan earthquakes that occurred between 2014 and 2018 and had ML magnitudes of 2.8 to 3.9 are identified in this study using spectral inversion. To construct the spectrum analysis code, the authors acquired the seismic analysis code (SAC) and MATLAB. We determined the source parameters (seismic moment, static stress drop, and source radius) and their scaling relations using the displacement source spectra from P-waves. If the activities in this area are technically created or caused by the Nasser Lake, it can be determined by comparison with regional cases using stress reduction. The main conclusion is that the source radius ranges from (407-790) m, the corner frequencies of the examined events range from (3.6-6.9) Hz, stress decrease, and (0.04-6.7) bar, and the seismic moment ranges from (3.22E+19-2.88E+21) dyne-cm. These results are mostly in agreement with earlier studies done in the same seismic zone. Although the anticipated stress declines are not depth-dependent, they can occasionally be greater where the N-S and E-W trend fault systems converge. However, reservoir-induced activity might have a low-stress drop when compared to earthquakes with tectonic origins.

Keywords: Aswan, seismicity, source parameters, seismic moment and stress drop

1. Introduction

Aswan is found in Upper Egypt, a stunning area of Egypt (Figure 1). It's situated between latitudes 23.00^0 and 24.00^0 N and longitudes 32.12^0 and 33.10^0. The importance of this area is mostly due to the hydroelectric project at the Aswan High Dam and historical sites. Egypt is debating how to safeguard this area from all threats, particularly earthquakes, both now and in the future.

Around the world, there are numerous research on the topic of source parameters (such as Aki, 1967; Brune, 1970; Madariaga, 1976; Hanks, 1977, among others). Measurements performed in the frequency domain are used to determine the source parameters. Kinematic and dynamic source models, for instance, predict the seismic moment from the low-frequency level ($\Omega_\circ$) of displacement spectra and the rupture length (radius of circular ruptures)

from the spectral corner frequency ($f_\circ$) (Brune, 1970; Madariaga, 1976). The results of this research support the significance of source characteristics for comprehending an area's seismotectonic. This in turn is regarded as a crucial component in the assessment of seismic risk.

This study's major goal is to build a list of improved earthquake source parameters from earlier research that sheds light on the topic and to estimate new ones for the eight occurrences chosen for this investigation. As a result, the scaling relations for the Aswan seismic zone will be improved and evaluated. To compare the results with those of other case studies in the Aswan region that have similar circumstances. As the region is thought to be a reservoir-triggered earthquake region (Haggag et al., 2009), it is assumed that the high pore pressure and the water-filled cracks will reduce friction along the area's causative faults, which will then

affect the physical characteristics of these   faults (seismic sources).
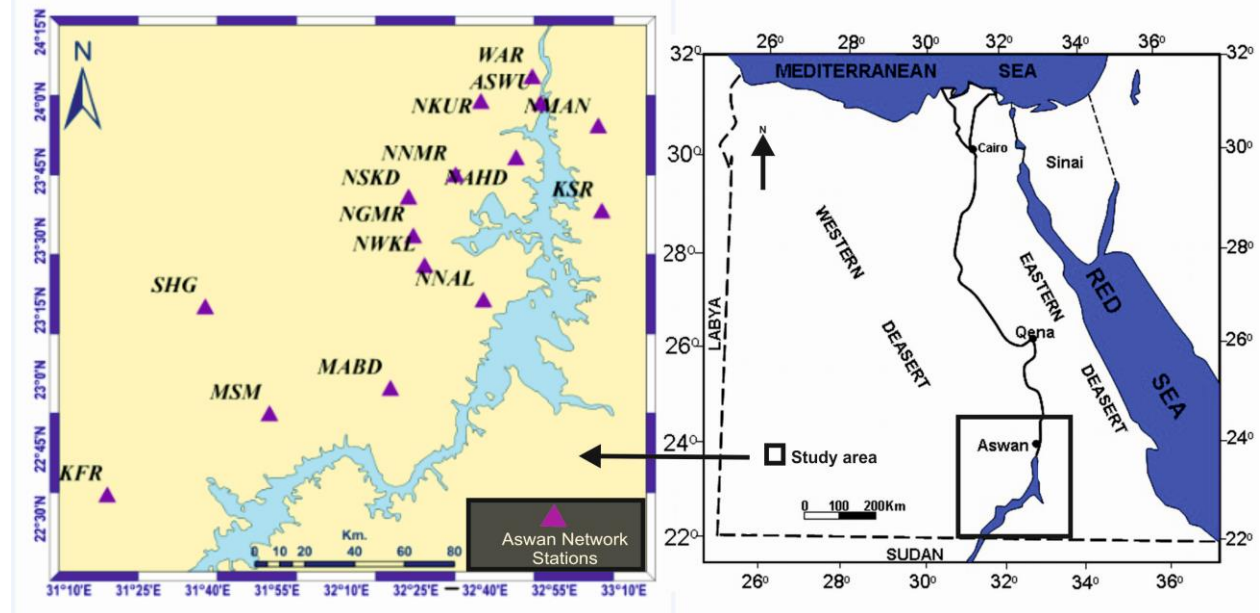
Figure 1: The Location map of the studied area (Right) and distribution of the Earthquakes' stations (Left).

2. Data and Source Model

Eight events that occurred between 2014 and 2018 and ranged in magnitude from ML 2.08 to 3.9 make up the data set analyzed in this study. The data of the selected earthquakes are a velocity waveform type collected by three components of broadband stations of the Aswan network; the location parameters of the examined events are provided in Table 1 and depicted in Figure 1 with the symbols of stations that caused them. These data are kept in a seed format with 100 samples per second. Keep in mind that source parameter estimation only uses the selected events that have at least five records. The time signal of the ground motion brought on by an earthquake is the seismic record. Convolution of the source effect, path effect, site reaction resulting from local geology, and instrumental impact yields the observed ground motion (i.e., record) in the time domain as follows:

$$U(t) = S_0(t) * Q(t) * R(t) * I(t) \quad (1)$$

Where $U(t)$ is the time series of observed ground displacement, $*$ denote the convolution, $S_0(t)$ is the ground notion of source, $Q(t)$ is the path attenuation model, $R(t)$ is the site response due to local geology, and $I(t)$ is the instrumental effect. The observed ground motion displacement spectrum, $U(f)$ can be represented in the frequency domain by multiplying the four physical parameters of eq. 3.1 as follows, using the Fast Fourier transform:

$$U(f) = S_0(f)\, Q(f)\, R(f)\, I(f) \quad (2)$$

By eliminating the instrumental response, site transfer function, and path effect, the true observed ground motion from the source is achieved as shown by the following relation:

$$S_0(f) = \frac{U(f)}{Q(f)R(f)I(f)} \quad (3)$$

The source model suggested by Boatwright (1978) is used to estimate source parameters and is expressed by the relation below:

$$d(f) = \frac{\Omega_o \, exp(-\pi f t^*)}{\sqrt{1 + (\frac{f}{f_0})^{2\gamma}}}$$

Alternatively, as follows in the log function form:

$$gammas \log(d(f)) = \log(\Omega_o) -$$

$$0.5 \, log\left[1 + \left(\frac{f}{f_0}\right)^{2\gamma}\right] - 0.434 \, (\pi f t^*) \quad (4)$$

where d (f) is the displacement spectrum, Ω0 is the low-frequency spectrum's amplitude

level, f0 is the corner frequency, t^* the attenuation parameter based on the quality factor Q, and the travel time, t (t^*=T/Q) and is a constant that regulates the corner's sharpness and is connected to the high-frequency decay. It is commonly known that a strongly attenuating site has small values of Q, whereas a weakly attenuating medium exhibits high values of Q.

Table 1 Relocation of the eight events of this study area

| Y M D H MI	Lat.(N)	Long.(E)	Dist. Error	Focal Depth (km)	Depth Error	Rms	Ml
2014 10 18 22 02	23.5811	32.7872	0.42	3.46	1.10	0.19	2.45
2015 11 21 10 47	23.5828	32.7747	0.47	9.11	0.97	0.21	2.91
2015 11 21 10 53	23.5795	32.7772	0.42	9.02	1.00	0.16	3.1
2016 09 19 21 50	23.5781	32.7229	0.50	9.21	1.49	0.16	3.6
2016 09 21 12 35	23.5771	32.7121	0.48	8.41	1.08	0.27	3.16
2017 01 14 08 50	23.5833	32.7102	0.65	9.65	1.65	0.29	2.5
2017 05 24 19 50	23.5741	32.7137	0.57	9.18	1.19	0.17	2.08
2018 01 22 16 20	23.5830	32.7811	0.55	11.63	1.54	0.28	3.3

3. Data analysis

Using the Rdseed application, which can be downloaded from the IRIS (Incorporated Research Institutions for Seismology) website, the waveform data of the eight earthquakes are transformed from seed format to SAC format. The observed waveform data are analyzed using the seismic analysis code (SAC Goldstein and Snoke, 2005) running under the UNIX operating system. Time windows of various lengths are investigated to choose one that prevents contamination from other phases achieves a good resolution and maintains spectral stability. Figures 2b to 5b depict a chosen window of 2 to 4 seconds that, in the first instance, contains the arrival time of the P-wave recovered from the vertical component of the record. The instrument response is then removed using the poles and zeros file of the stations after the mean and linear trend have been removed. The Q value is eliminated after using the broadband

filter. The signal is then transformed using the Fast Fourier Transform (FFT) to create a spectrum, or a Fourier spectrum, which is a representation of the time-domain signal in the frequency domain. The integration procedure (i.e., dividing by ω) transforms the velocity data into a displacement. Finally, the output displacement spectrum is obtained from the output amplitude spectrum (logarithmic plot of the amplitude spectrum), the output spectrum is saved as depicted in figures 2c to 5c, and the values of the corner frequency ($f_\circ$) and the long period spectral level flat part, $\Omega_\circ$ (f $\ll f_\circ$), are found there (Table 2). Then, using the nonlinear least squares inversion technique, the theoretical source model of Boatwright's (1978) equation (3.4) is estimated using MATLAB software. The best fit between the estimated and observed displacement amplitude spectra of P-waves, as determined by SAC software, is shown in Figure 3.6.
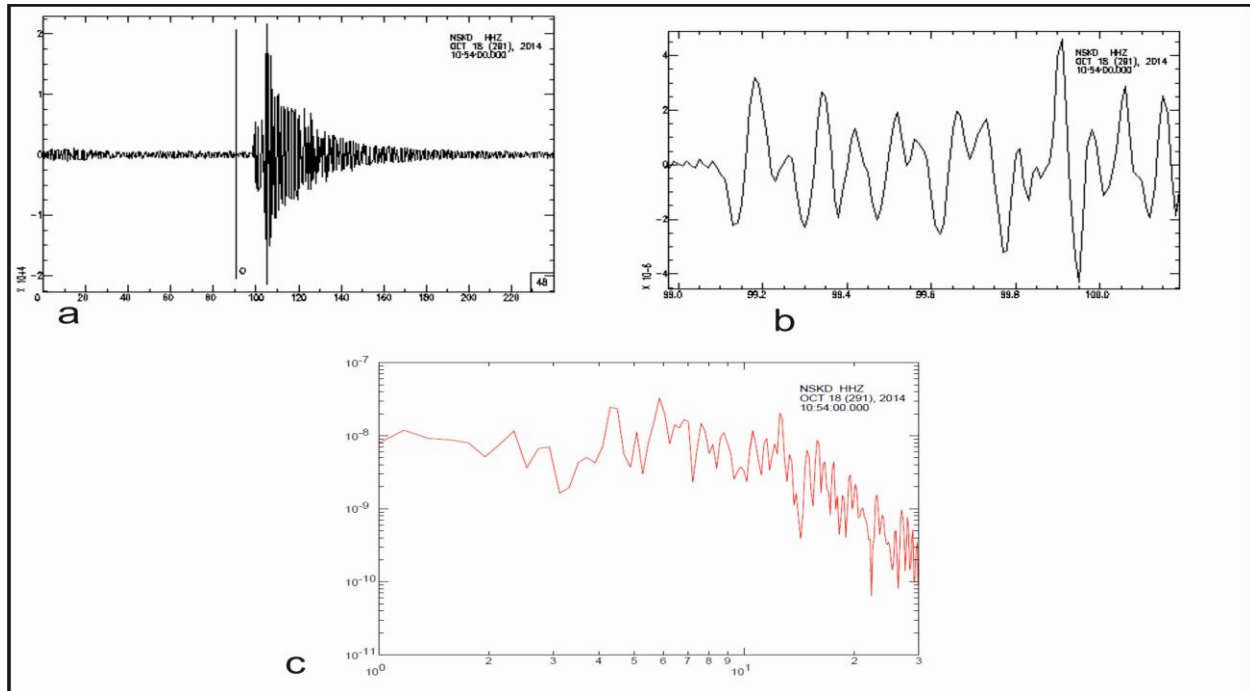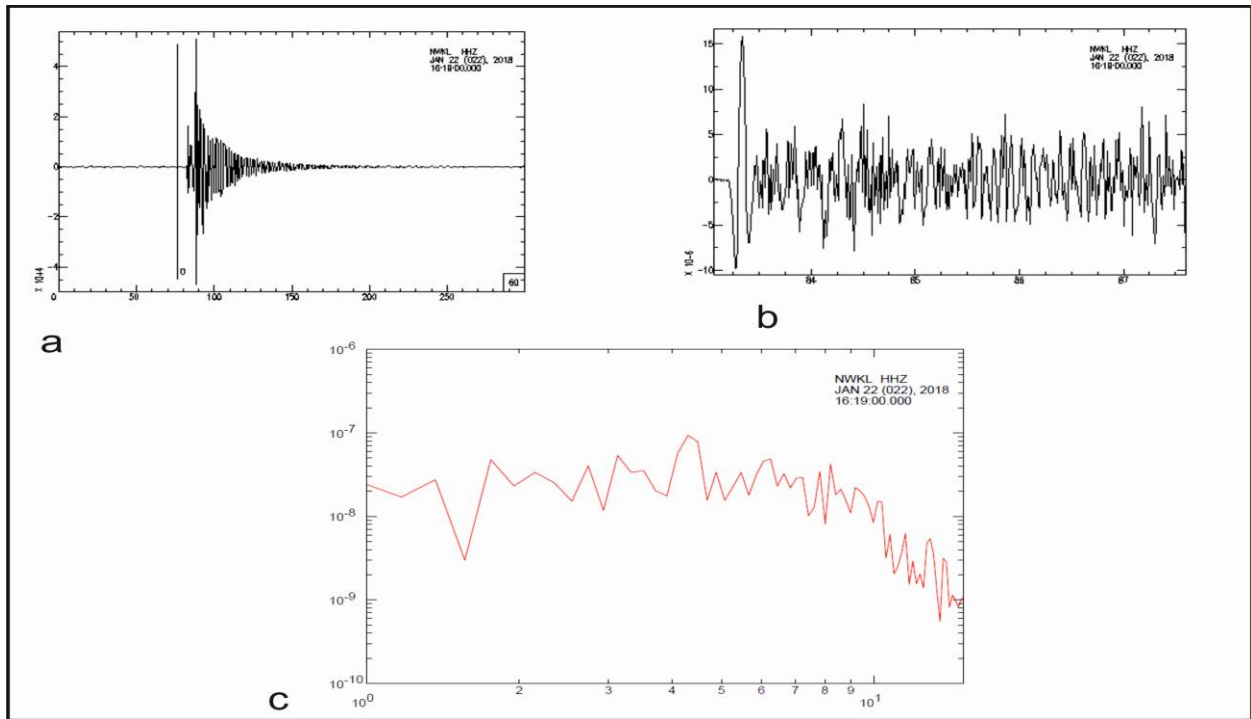
Figure 2: Example from the NSKD station to the first event (18 October 2014). The vertical component of the extracted waveform's P-wave's arrival time is shown in (a), the time window employed is shown in (b), and the output logarithmic spectrum is shown in (c).
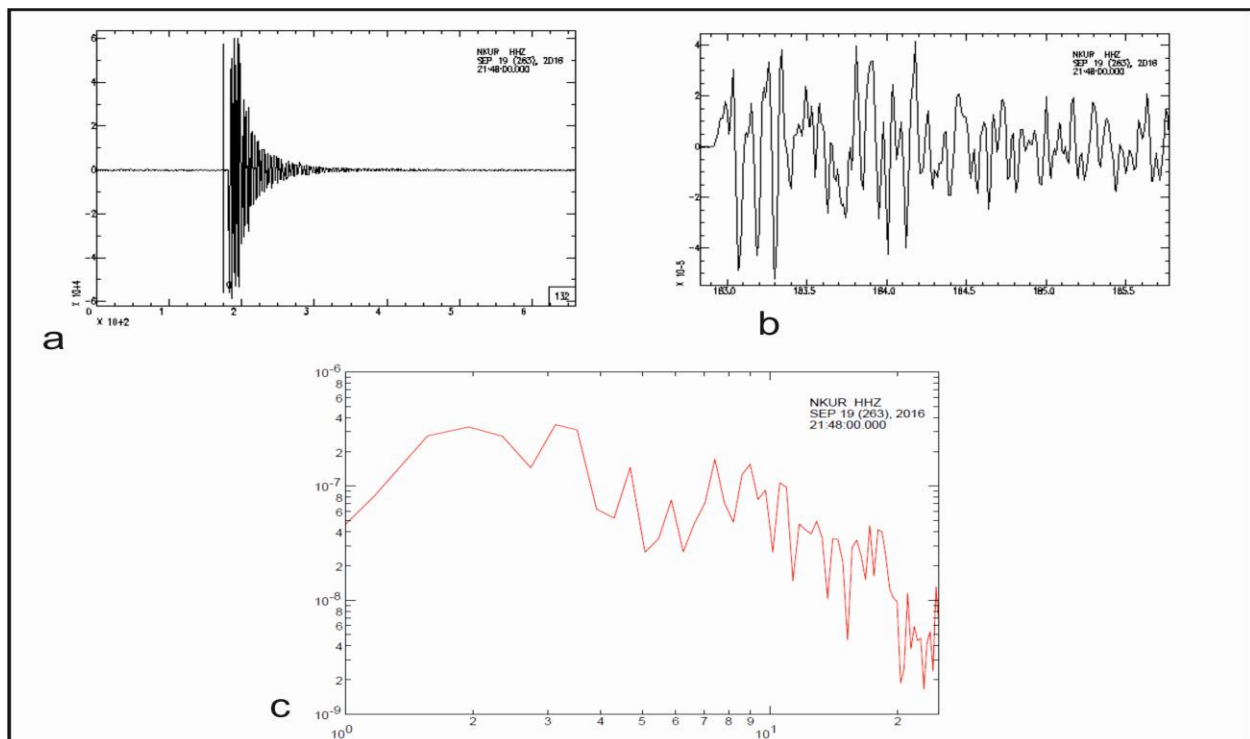
Figure 3: Example of event No. 4 from NKUR station (19/09/2016). The vertical component of the extracted waveform's P-wave's arrival time is shown in (a), the time window employed is shown in (b), and the output logarithmic spectrum is shown in (c).
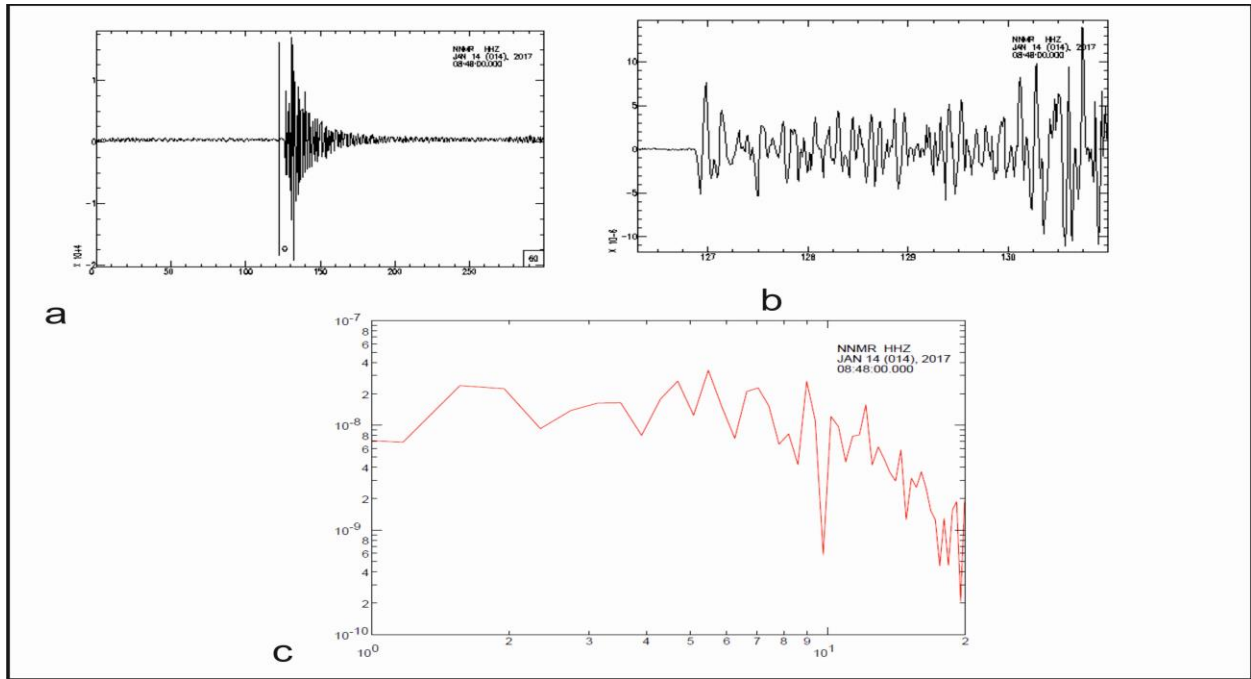
Figure 4: Example of event No. 6 from the NNMR station on January 14, 2017. The vertical component of the extracted waveform's P-wave's arrival time is shown in (a), the time window employed is shown in (b), and the output logarithmic spectrum is shown in (c).

Figure 5: Example of event no. 8 from NWKL station on January 22, 2018. The vertical component of the extracted waveform's P-wave's arrival time is shown in (a), the time window employed is shown in (b), and the output logarithmic spectrum is shown in (c).

4. Source parameters determination

Once we know the corner frequency ($f_\circ$) and the long-period flat section of the spectral level, we may use the spectral inversion method (i.e., P-wave displacement spectra) to determine these values. It's time to calculate the source characteristics for the selected events, including the stress drop ($\Delta\sigma$), seismic moment ($M_\circ$), fault radius ($r_\circ$), displacement across the fault ($d_\circ$,), and moment magnitude (M_w). The following circular source model corresponds to the values of these parameters, which were determined from relations by Brune (1970& 1971), Hanks and Ways (1972), and Kanamori (1977):

$$M_o = \frac{4\pi\rho v_p^3 * \Omega_o}{F*R\theta\phi*G(r,h)} \tag{5}$$

$$r_o = \frac{2.34v_p}{2\pi f_o} \tag{6}$$

$$\Delta\sigma = \frac{7M_o}{16r_o^3} \tag{7}$$

$$d_o = \frac{M_O}{\pi\rho V_s^2 r_o^2} \tag{8}$$

$$M_w = 2/3 \; \log_{10}(M_o) - 10.7 \tag{9}$$

Where M_0 is a seismic moment, p is the medium's density, and Vp is the P-wave's velocity calculated using a crustal model in Table 2 based on the depth of the earthquake. Geometrical spreading is denoted by the notation G (r, h), where (*r*) **is** the epicentral distance and (*h*) focal depth. The symbols f is the frequency, f_o is the corner frequency, and the observed flat level (Ω_0). F reveals to be a free surface effect and is calculated for each station using FOCMEC from the value of V_P/V_S and the emergence angle of P and S waves. For P-waves, it is assumed that the radiation pattern, $R\theta\phi$ has an average value 0.52 (Boore and Boatwright 1984 & Aki and Richards 2002).

Table 2: Aswan seismic velocity model, P and S velocity (km/sec) and Depth (km)

P-velocity (km/sec)	Depth (km)	S-velocity (km/sec)
4.00	0.00	2.30
6.00	0.50	3.40
6.80	5.00	3.90
7.50	20.00	4.30

According to Archuleta et al. (1982) relation, the average value for each parameter is calculated for each event from individual stations:

$$X = \text{anti} \log(\frac{1}{N_s}\sum_{i=1}^{N_s} \log X_i) \tag{10}$$

The total number of stations used is Ns, where X is any parameter.
The following equations are used to determine the standard deviation (i.e., uncertainty) and multiplicative error factor (E_x).

$$SD(\log\langle x\rangle) = [\frac{1}{N_s-1}\sum_{i=1}^{N_s}(\log X_i - \log\langle x\rangle)^2]^{.5} \tag{11}$$

$$E_x = \text{anti} \log SD(\log\langle x\rangle) \tag{12}$$

5. Results

To determine the source parameters of Aswan earthquakes of magnitudes between ML (2.08 and 3.6) from 2014 to 2018, spectral inversion is used. Brune's omega squared source model, which is based on the spectral analysis technique discussed above, will aid in identifying the source parameters, including a flat part (Ω_0) spectrum and a corner frequency ($f_\circ$), which is located where high and low frequencies converge. The seismic moment M, which is the source strength, stress drop ($\Delta\sigma$), which is the difference between shear stress before and after an earthquake on the fault surface (Prochazkova, 1976 & 1980), and source radius ($r_\circ$) is then computed using the two parameters. The following parameters are obtained from equations 5 to 12:

5.1 Seismic moment M_o

The Seismic Moment (M_o), which is referred to as a static source parameter since it depends on the conditions before and after earthquakes but not on the actual time history of faulting, is regarded as the most accurate measurement of an earthquake's size (Kanamori and Brodsky 2004). Individual stations estimate it using equation 5; the derived average value then corresponds to each event, and its

uncertainty is calculated using equations 10 to 12. The eight events that were studied yielded values that ranged from 2.23E+19 to 1.48E+21 dyne-cm.

5.2 Source radius (r_o)

The values of V_P and corner frequency (f_o) observed at each station can be substituted into equation 6 to estimate the source radius (r_o). The average value and the degree of uncertainty are then also determined (Tables 3 and 4). As per the kinematic model of Brune (1970) for a circular defect (eq. 6), it is widely known that the corner frequency is inversely proportional to the source radius. The point where the low-frequency and high-frequency portions of the source spectra converge is known as the corner frequency (Lay and Wallace 1995). From amplitude spectrum displacement, corner frequency has been discovered. The eight events were examined, with the source ranging from (393-783) m in radius and a corner frequency of (3.5-6.8) Hz.

5.3 Displacement across the fault (d_o)

In addition, the seismic moment, shear wave velocity, and rupture radius are used to determine the displacement across the fault (d_o) (see equation 7). The average value is between 0.002 and 0.25 cm.

5.4 Stress drop (Δσ):

In the faulting process, the stress drop (Δσ) is the most important. Numerous research (e.g., Kanamori, 1981; Zobin et al., 1984) indicates that this parameter is one of the factors that determine the amplitude of the ground acceleration produced by the earthquake. The differential in the stress level at a spot on the fault before and after rupture is what causes a rupture. A measurement of the change in stress between the time before an earthquake and the time after the fault has ruptured is called the static stress drop. With the seismic moment M_0 and the source radius $r_\circ$, one can use Eshelby's (1957) equation (4) to determine the stress drop drop (Δσ) for a circular fault rupture. The stress drop ranges from 0.02 to 3.56 MPa, but the mean and median values in response to the eight events are only 0.96 and 0.72 MPa, respectively.

Accordingly, the stress drop is utilized to determine, by a comparison with the regional cases, whether the activity in this location is tectonic in origin or produced because of the Nasser Lake. According to Sadalla et. al. (2019), Sadalla et. al. (2020), Abercrombie and Leary (1993), Fehler and Philips (1991), Gibowicz et al., (1991), and Mandal et al., (1998), the results of this study support the hypothesis that reservoir-induced seismicity appeared to have a lower stress drop than tectonic earthquakes.

5.5 Moment magnitude M_W

Finally, using Kanamori's (1977) relation and equation 9, the moment magnitude is computed. The Mw parameter scale has the advantage of being tied to the source's physical characteristics and not saturation for even the greatest earthquakes.

Tables 2 and 3 contain a list of the eight events that were evaluated in this study's source parameters. According to the relation given by Archuleta et al. (1982), Table 4 contains the average values (x) calculated from Table 3 for each parameter. The results are in conformity with earlier research done in this seismic region.

Table 3: Source parameters for all stations.

Event no.	St.code	Δ (km)	f_o (Hz)	Ω_o (Cm s)	M_o (dyne/cm)	r_o (m)	$\Delta\sigma$(Mpa)	d_o (cm)	M_w
1	NGRW	9.7	4	3.00E-7	3.64E+18	633	.006	.001	1.6
	NAHD	24.5	11	2.00E-7	6.13E+18	230	.219	.008	1.8
	NKUR	48.9	6	9.00E-7	5.51E+19	422	.319	.022	2.4
	NMAN	47.3	7	3.00E-7	1.78E+19	362	.163	.009	2.1
	NNMR	28.8	6	9.00E-6	3.24E+20	422	1.88	.131	2.9
	NSKD	41.9	7	1.00E-7	5.24E+18	362	.048	.003	1.7
	NWAL	30.6	5.8	9.00E-6	3.45E+20	437	1.80	.130	3
	NGMR	39.3	6.5	2.00E-7	9.84E+18	390	.072	.005	1.9
2	KSR	32	5.3	9.00E-6	5.23E13	527	1.56	.104	3.1
	MABD	81.7	4.5	5.00E-7	7.42E19	621	.135	.010	2.5
	NGAL	18.6	7	8.00E-6	2.70E20	399	1.85	.094	2.9
	NGRW	9.6	6	9.00E-7	1.57E19	466	.067	.004	2.1
	NNAL	34	5.5	7.00E-6	4.32E20	508	1.44	.093	3
	NNMR	27.7	5	6.00E-6	3.02E20	559	.756	.053	2.9
	NSKD	40.6	5.8	5.00E-6	3.69E20	482	1.44	.088	3
	NWKL	38.2	5	7.00E-6	4.85E20	559	1.21	.086	3.1
3	NGMR	38.4	6.5	9.00E-6	6.27E+20	430	3.45	.188	3.1
	NNAL	33.7	5	9.00E-6	5.51E+20	559	1.37	.097	3.1
	NNMR	28.1	7.8	9.00E-6	4.59E+20	358	4.36	.198	3.0
	NSKD	40.9	6	8.00E-6	5.94E+20	466	2.57	.152	3.1
	NWKL	38.3	7.5	1.00E-6	6.95E+19	373	0.58	.027	2.5
	KSR	31.8	9	9.00E-7	5.20E+19	311	0.75	.029	2.4
4	KSR	37.4	5	4.00E-6	2.72E+20	559	0.68	.048	2.9
	NGMR	32.8	4.8	9.00E-5	5.36E+21	582	11.8	.878	3.8
	NKUR	47.7	4.5	1.00E-6	8.66E+19	621	0.15	.012	2.6
	NMAN	51.8	6	8.00E-6	7.52E+20	466	3.25	.192	3.2
	NNAL	32.1	4.8	9.00E-5	5.24E+21	582	11.6	.859	3.7
	NNMR	24.1	4.7	6.00E-5	2.63E+21	595	5.46	.412	3.5
	NSKD	35.6	4.8	5.00E-5	3.23E+21	582	7.16	.529	3.6
	NWKL	33.4	5	9.00E-5	5.46E+21	559	13.6	.970	3.8
5	KSR	38.5	5	9.00E-6	6.29E+20	559	1.57	.111	3.1
	MABD	77.7	3.5	8.00E-6	1.13E+21	798	0.96	.098	3.3
	NGMR	31.7	4.6	7.00E-6	4.03E+20	608	0.78	.060	3.0
	NKUR	47.7	7	4.00E-6	3.46E+20	399	2.38	.120	3.0
	NMAN	52.7	6	3.00E-7	2.87E+19	466	0.12	.007	2.2
	NNAL	31.8	4	6.00E-6	3.46E+20	699	0.44	.039	3.0
	NNMR	23.5	4.5	9.80E-5	4.18E+21	621	7.63	.602	3.7
	NSKD	34.5	4	2.00E-6	1.25E+20	699	0.16	.014	2.7
	NWKL	32.4	3.5	8.00E-6	4.71E+20	798	0.40	.041	3.1
6	KSR	38.6	3.2	8.00E-7	5.61E+19	873	0.03	.004	2.4
	NGMR	31.7	3.2	3.00E-7	1.73E+19	873	0.01	.001	2.1
	NMAN	52.3	4	8.00E-7	7.60E+19	699	0.09	.008	2.5
	NNAL	32.5	4	2.00E-7	1.18E+19	699	0.01	.001	2.0
	NNMR	22.8	4	1.00E-7	4.14E+18	699	0.01	.001	1.7

Event no.	St.code	Δ (km)	f_o (Hz)	Ω_o (Cm s)	M_o (dyne/cm)	r_o (m)	$\Delta\sigma$(Mpa)	d_o (cm)	M_w
	NSKD	34.2	8	3.00E-7	1.86E+19	349	0.19	.008	2.1
	NWKL	32.7	2.6	7.00E-7	4.16E+19	107	0.014	.002	2.3
	KSR	38.3	4	9.00E-7	6.26E+19	699	0.08	.007	2.5
	NGMR	31.8	4	7.00E-7	4.04E+19	699	0.05	.004	2.3
7	NMAN	52.8	3.2	9.90E-7	9.49E+19	873	0.06	.006	2.6
	NNAL	31.5	3	6.00E-7	3.43E+19	932	0.01	.002	2.3
	NSKD	34.8	4.2	1.00E-7	6.32E+18	665	0.01	.000	1.8
	NWKL	32.4	3.2	7.00E-7	4.12E+19	873	0.02	.003	2.3
	KSR	31.4	4	9.00E-6	5.13E+20	699	0.65	.058	3.1
	NGMR	38.8	3.8	7.00E-6	4.93E+20	735	0.54	.050	3.1
8	NKUR	48.5	3.8	6.00E-6	5.28E+20	735	0.58	.054	3.1
	NNMR	28.2	4.9	8.00E-6	4.10E+20	570	0.96	.070	3.0
	NSKD	41.2	4	7.00E-6	5.24E+20	699	0.67	.059	3.1
	NWKL	38.8	4.8	9.00E-6	6.34E+20	582	1.40	.103	3.1

Table 4: The estimated seismic moment, fault radius, stress drop, moment magnitude, and average displacement as determined from Table (3) are represented by the average values (AV) of the source parameters, the standard deviation (SD), and the multiplicative error factor (Ex).

Event no.	f_o (Hz)	Ω_o (Cm s)	M_o (dyne/cm)	r_o (m)	$\Delta\sigma$(Mpa)	M_w	d_o (cm)
1 AV	6.43 ±0.1	2.50E-06	2.44E+19	393	0.174	2.19	0.011
SD			±0.7	±0.1	±0.8	±0.1	±0.7
Ex	1.3		6.1	1.3	6.6	1.2	6.2
2 AV	5.46	5.43E-06	2.10E+20	511	0.689	2.81	0.044
SD	±0.05		±0.5	±0.05	±0.5	±0.05	±0.6
Ex	1.1		3.3	1.1	3.5	1.1	4.5
3 AV	6.84	6.15E-06	2.64E+20	408	1.697	2.88	0.088
SD	±0.09		±0.5	±0.09	±0.3	±0.05	±0.3
Ex	1.2		3.1	1.2	2.2	1.1	2.4
4 AV	4.93	4.91E-05	1.48E+21	566	3.562	3.38	0.25
SD	±0.03		±0.6	±0.03	±0.5	±0.06	±0.6
Ex	1.08		4.8	1.08	3.5	1.1	4.8

Event no.	f_o (Hz)	Ω_o (Cm s)	M_o(dyne/cm)	r_o (m)	$\Delta\sigma$(Mpa)	M_w	d_o(cm)
5 AV	4.55	1.58E-05	3.96E+20	612	0.753	3.00	0.058
SD	±0.1		±0.5	±0.1	±0.5	±0.05	±0.6
Ex	1.2		3.9	1.2	3.6	1.1	4.5
6AV	3.89	4.57E-07	2.23E+19	717	0.026	2.16	0.002
SD	±0.15		±0.4	±0.1	±0.5	±0.06	±0.4
Ex	1.4		2.7	1.4	3.5	1.1	2.9
7AV	3.56	6.65E-07	3.59E+19	783	0.032	2.30	0.003
SD	±0.06		±0.4	±0.06	±0.3	±0.05	±0.3
Ex	1.1		2.5	1.1	2.2	1.1	2.2
8 AV	4.19	7.67E-06	5.12E+20	666	0.757	3.07	0.064
SD	±0.5		±0.06	±0.05	±0.1	±0.005	±0.1
Ex	1.1		1.1	1.1	1.4	1.0	1.2
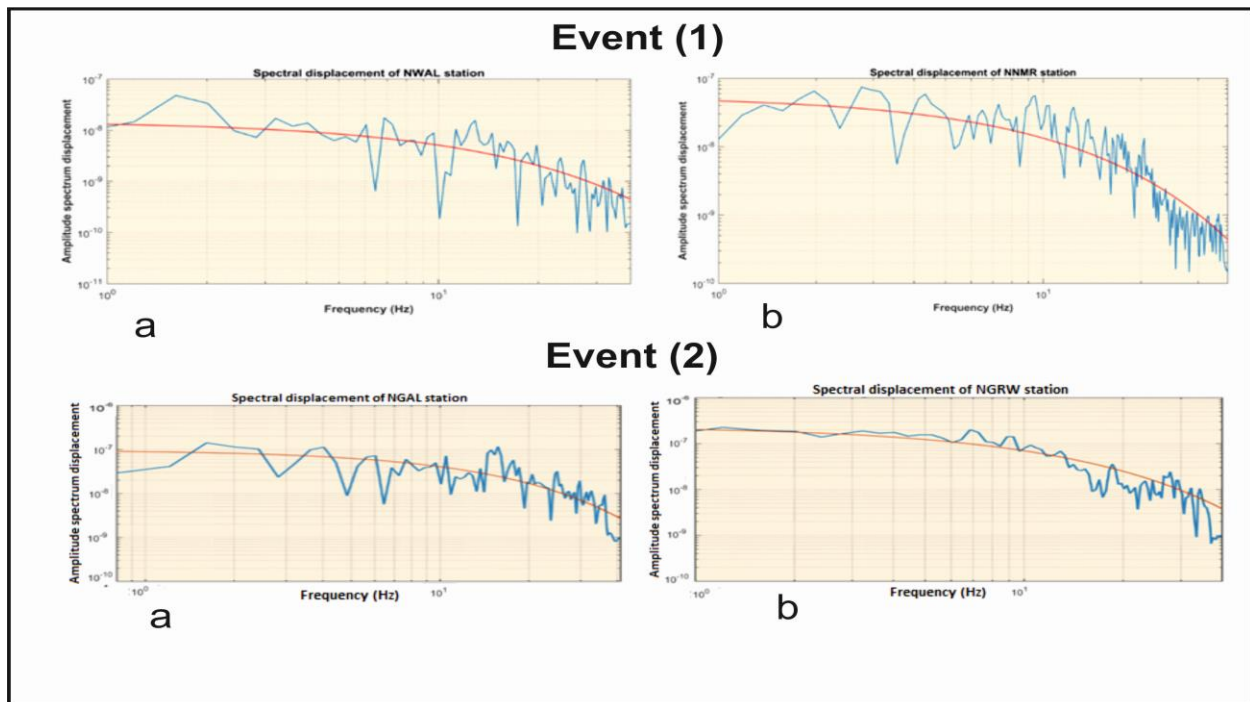
Figure 6: Displacement amplitude spectra for event no. 1(recorded by NWAL station, and NNMR station) and event no. 2 (recorded by NGAL station and NGRW station).
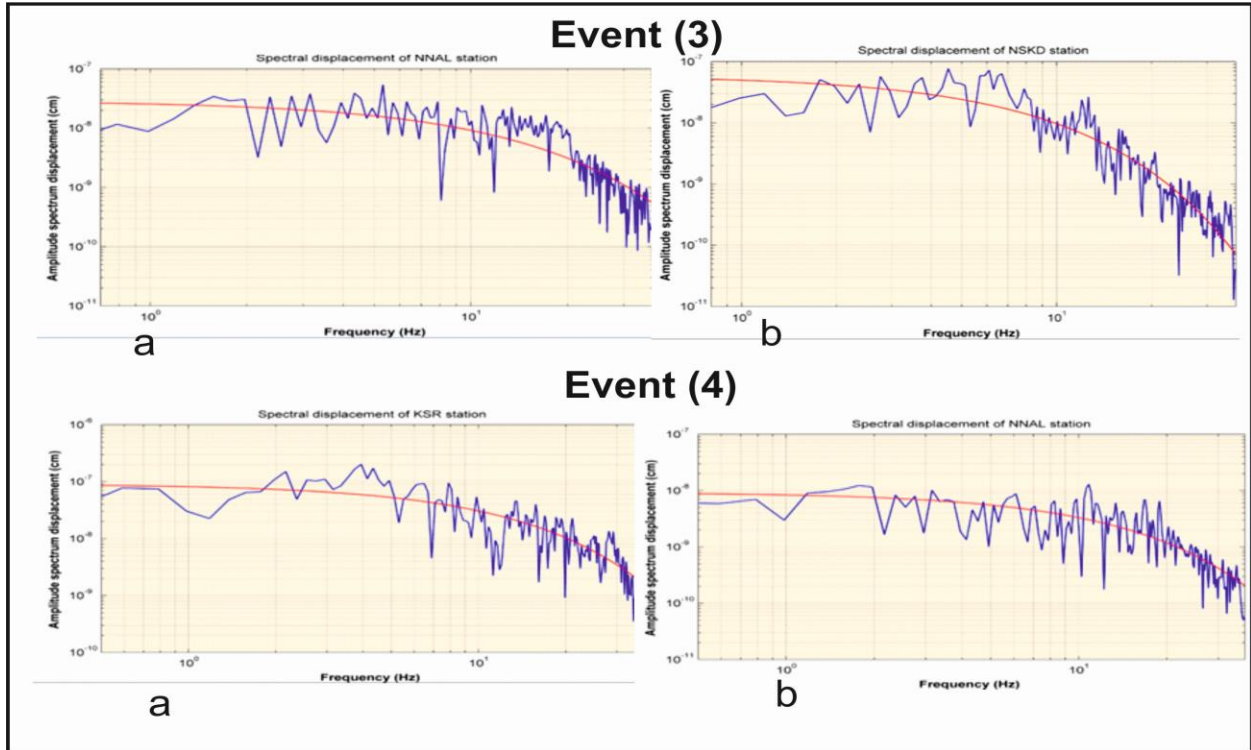
Continue figure 6: Displacement amplitude spectra for event no. 3(recorded by NNAL station, and NSKD station) and event no. 4 (recorded by KSR station, and NNAL station).
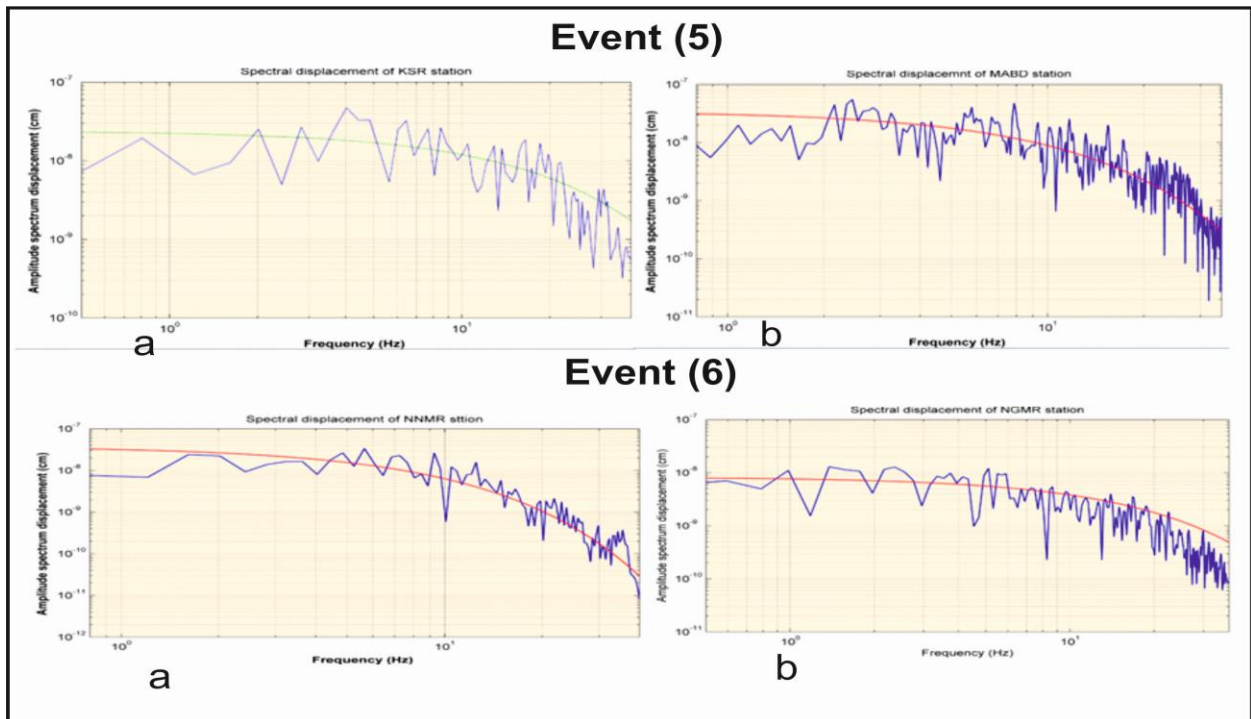
Continue Figure 6: Displacement amplitude spectra for event no. 5 (recorded by KSR station and MABO station) and event no. 6 (recorded by MNMR station and NGMR station).
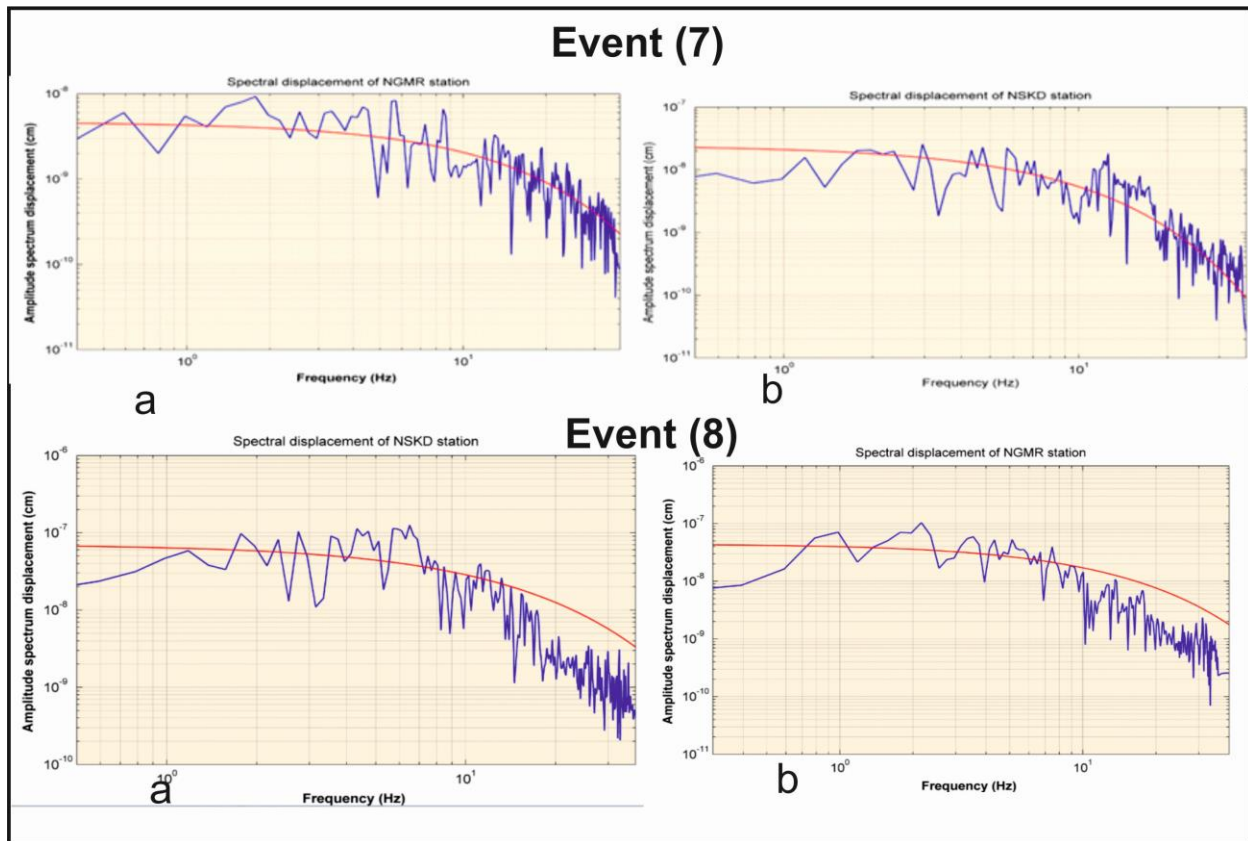
Continue figure 6: Displacement amplitude spectra for event no.7 (recorded by NGMR station, and NSKD station) and event no. 8 (recorded by NSKD station and NGMR station).

6. Scaling relations

The empirical relationship is formed and updated from the point of view of all data based on the data in Table 4 that were produced from this study and those collected from prior work. In several areas of seismology, scaling laws for earthquake source parameters are applied. The relationship between the various earthquake source parameters is described by these scaling equations. Before using source characteristics, such as stress drop, for earthquake prediction, the scaling equations of earthquakes must be established. Some studies have tried to identify regional or temporal differences in stress drop as markers of changes in the amount of tectonic stress. The significance of such changes in stress drop can only be assessed after the relationship between stress drop and the seismic source.

The scaling relationship between the various earthquake source parameters, including seismic moment - local magnitude $(M_o - M_l)$, seismic moment - source radius $(\log M_o - \log r_\circ)$, seismic moment - stress drop $(M_o - \Delta\sigma)$, moment magnitude - local magnitude $(M_w - M_l)$, corner frequency-local magnitude $(fo - M_l)$, stress drop – depth and corner frequency-seismic moment $(fo-M_o)$ will be determined in this study. Without the need to run any spectral analysis programs, the scaling relations will aid in the quick computation of the various source parameters for the earthquakes in the region.

- **Seismic Moment and Source Radius**

The empirical relation between the seismic moment of *P*-wave *(log M_o)* and the source radius *(log r_o)* is obtained as shown in figure 7 in the following linear relation: -

$$\text{Log } M_o = 14.5 + 1.9 \log r_o$$
$$(13)$$
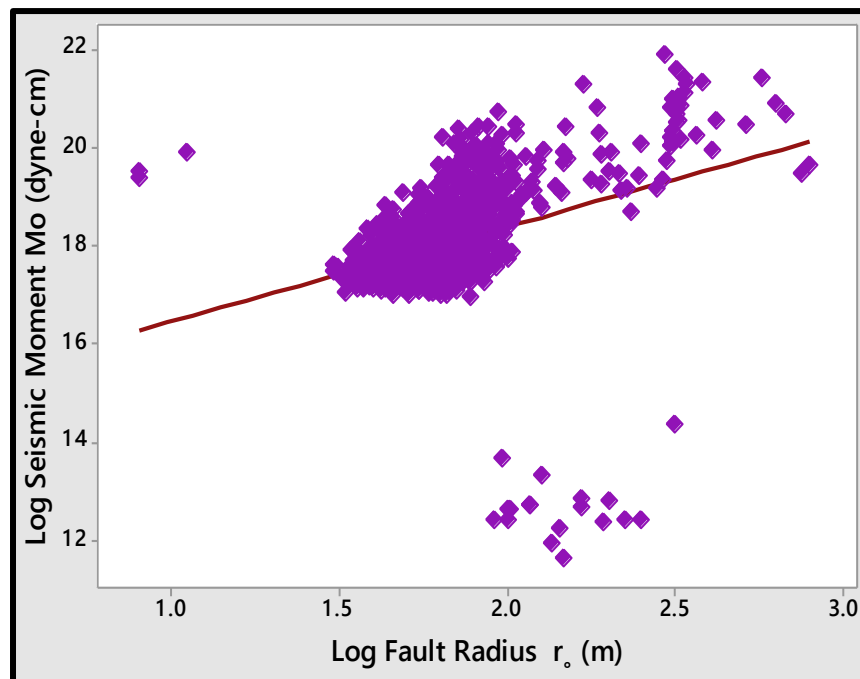
Figure 7: Linear relation between the Seismic Moment and Fault Radius.

- **Seismic Moment and Stress Drop**

Figure (8) calculates and plots the relationship between the seismic moment (log M_o) and the stress drop. The following empirical equation (15) results from the data's linear least-squares fit: -

$$\text{Log } M_o = 17.7 + 0.9 \log \Delta\sigma \qquad\qquad (15a)$$
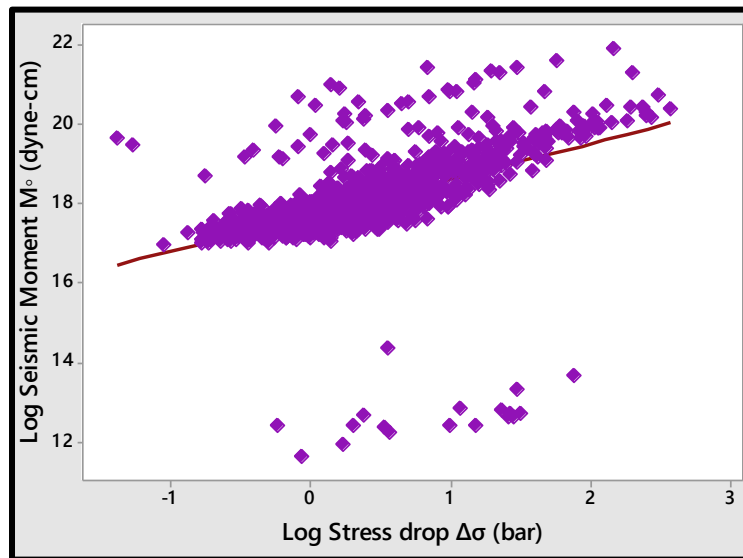
Figure 8: Linear relation between the Seismic Moment and Stress Drop.

- **Seismic Moment and Corner frequency**

Figure 9 illustrates the relationship between the seismic moment (**log M_o**) and corner frequency (**log f_o**). The data's linear least-squares fit yields the following empirical relationship: -

$$\text{Log } M_o = 21.6 - 2.8 \log f_o \qquad\qquad (15b)$$

According to the equation, the corner frequency and seismic moment have a reverse proportional relationship in which $Mo \approx f_o^{-2.8}$, or the corner frequency decreases as the seismic moment increases. Additionally, this relationship somewhat agrees with the scaling rule of earthquake self- similarity ($Mo \approx f_o^{-3}$).
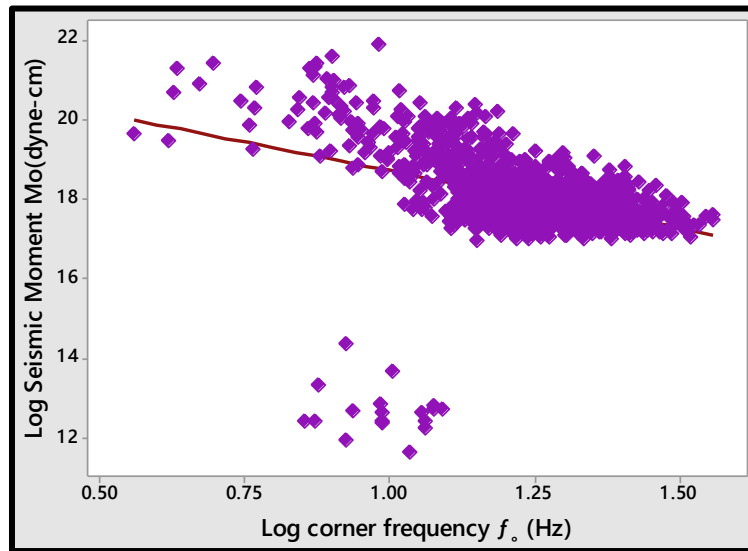
Figure 9: Linear relation between the Seismic Moment and Corner Frequency.

- **Corner frequency and Local magnitude**

Figure 10 shows the estimated and plotted relationship between the local magnitude (*Ml*) and corner frequency (**log** f_o). The following empirical equation results from the data's linear least-squares fit: -
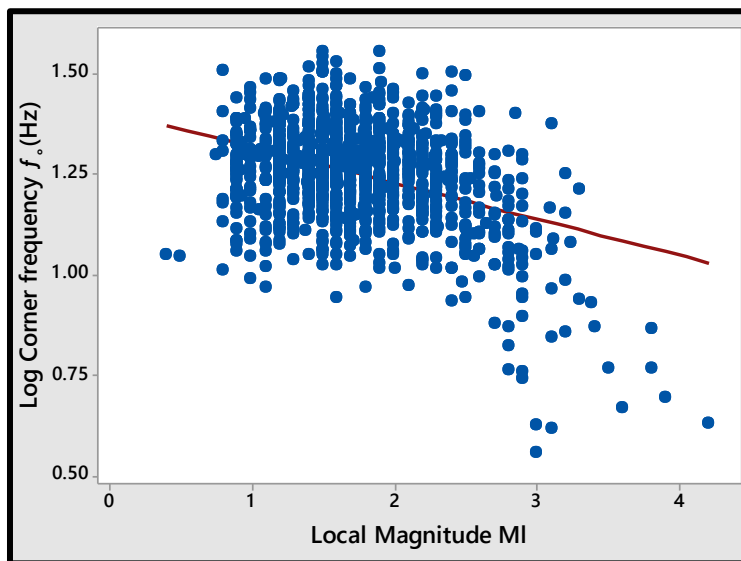
$$\text{Log } f_o = 1.40 - 0.08 \text{ Ml} \qquad\qquad (15c)$$

Figure 10: Linear relation between Corner Frequency and Local Magnitude.

- **Seismic Moment and Local Magnitude Relation**

Since it quantifies a component of the widely recognized earthquake source model, the seismic moment M_o is essentially superior to any magnitude scale. One limitation of M_o is the difficulty it is to accurately process seismic information on a large routine scale to calculate the magnitude of a seismic event. Numerous magnitude scales have been proposed for this purpose.

The energy radiated over a specific frequency range is quantified by magnitude (e.g., Aki, 1967). Since the frequency distribution of seismic energy changes in earthquake size, the magnitude scales are subject to inherent limits, including saturation and differences between different scales (e.g., Hanks and Kanamori, 1979).

The empirical relationships between the seismic moment and magnitude have always been expressed as a linear relationship between log M_o and the magnitude, as seen in the following equation:

$$\text{Log } (M_{o)} = a (M_m) + b \tag{16}$$

Whereas a and b are constants (i.e., the coefficients of the linear regression relation) and M_m is any magnitude scale. Figure (11) in this study illustrates the relationship between the M_l and the logarithmic seismic moment M_o values for P waves. Equation: The following empirical relation emerged:

$$\text{Log } M_o = 16.71 + 0.76 \text{ Ml} \tag{17}$$
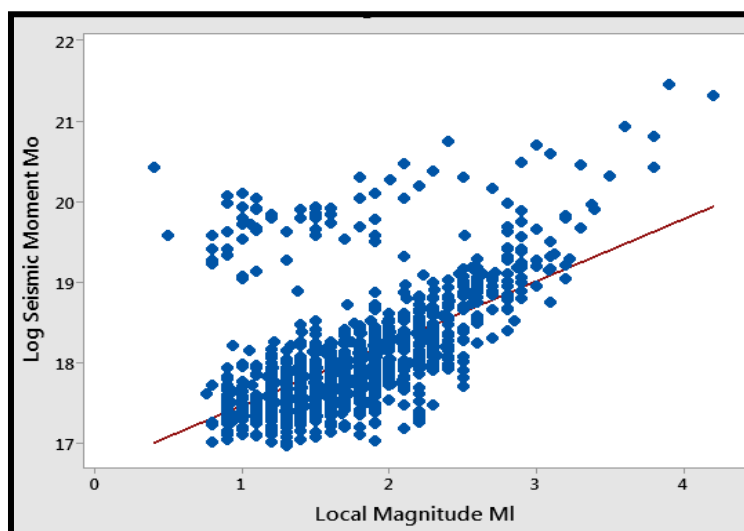
Figure 11: Linear relation between the Seismic Moment and Local Magnitude.
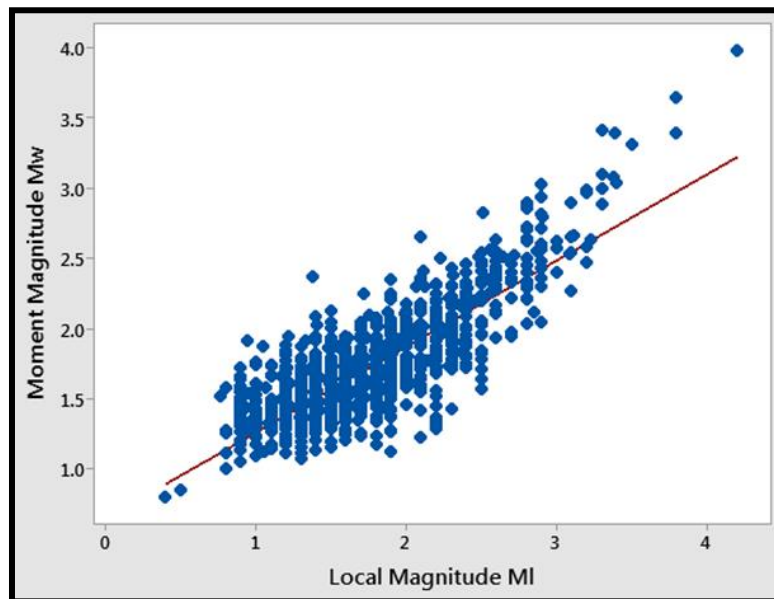
- **Moment Magnitude and Local magnitude**

The moment magnitude M_w, rather than the seismic moment itself, has increasingly been utilized to gauge earthquake power in recent years. Hanks and Kanamori (1979) formula provided a formal definition of this as follows: -

$$Mw = 2/3 \log M_o - 10.73 \qquad (18)$$

The Mw values that are provided in this investigation are displayed versus M_L Figure (12). The following is how the empirical relationship is found: -

$$Mw = 0.64 + 0.61 Ml \qquad (19)$$

We can get Mw values from this empirical relation that weren't cataloged in the earlier investigations.

Figure 12: Linear relation between Moment Magnitude and Local Magnitude.

- **Stress Drop and Depth Relation**

The stress drop doesn't appear to have a clear relationship with the depth of events, according to the plot of stress drops as a function of depth for the entire dataset (Figure 13), however the higher stress drop is occasionally found at the intersection of the N-S and E-W trend fault systems. However, when compared to earthquakes with tectonic origins, reservoir-induced activity could show a low-stress decline.
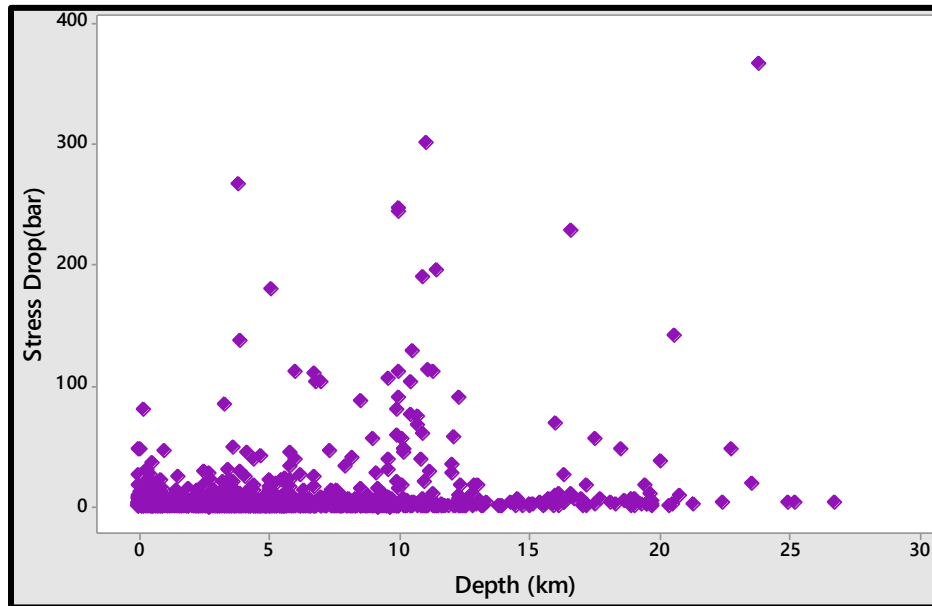
Figure 13: Relation between Stress Drop and Depth.

Conclusion

The digital waveform data used in this investigation were taken from the Egyptian National Seismological Network (ENSN). This data includes earthquakes that happened in the Aswan region between 2014 and 2018, with local magnitude (Ml) ≥ 2.8.

According to Brune's model of the omega square, spectral inversion is used for Aswan earthquakes to estimate corner frequency (f$_\circ$) and the long period spectral level (flat part). However, we can determine the seismic moment (M$_\circ$), displacement across the fault (d$_\circ$), fault radius (r$_\circ$), and moment magnitude (Mw) for the circular source model from the displacement spectra of p-waves.

Three steps are used at this stage. The first step is to use Rdseed to convert earthquake data from seed format to sac format. The second one is the seismic analysis code (SAC) that runs on the UNIX operating system and is used to determine when the P-wave will arrive in the vertical component. Finally, various equations were used to determine the values, and the results were illustrated using MATLAB software.

The main results are:

•   The seismic moment (**M$_o$**) for P -P-source spectra ranges from 2.23E+19-1.48E+21 dyne-cm.

• $f_\circ$ (Hz) corner frequency range from 3.5 to 6.8

• $\Omega_\circ$ (Cm s) flat part varies from 1.58E-05 - 6.65E-07

•   r$_\circ$ (m) source radii range from 393 to 783

• $\Delta\sigma$ (MPa) stress drop is 0.02-3.5

•   M$_w$ moment magnitude varies from 2.19 to 3.38.

Although there is no clear relationship between the anticipated stress decrease and depth, it can occasionally be higher where the N-S and E-W trend fault systems converge. Through a comparison with the regional cases, the stress decrease is used to determine if the activities in this location are tectonically produced or caused by the Nasser Lake. It may be confirmed by the

lower stress drop values found in this work that the reservoir-induced earthquakes have a lower stress drop.

Acknowledgment

References

[1] **Abercrombie, R., Leary, P. (1993).** Source parameters of small earthquakes recorded at 2.5km depth, Cajon Pass, southern California: implications for earthquake scaling. Geophys. Res. Lett, 20(14), 1511-1514.

[2] **Aki, K. (1967).** Scaling law of seismic spectrum. *Journal of Geophysical Research*, 72(4), 1217-1231.

[3] **Aki, K. and Richards, P.G. (2002).** Quantitative Seismology, vol. 1.

[4] **Archuleta, R.J., E., Cranswinck, CH., Mueller, and Spudich, P. (1982).** Source parameters of 1980 Mammoth lakes, California. Earthquakes sequence, J. Geophys. Res. 87, 4595-4607.

[5] **Boatwright, J. (1978).** Detailed spectral analysis of two small New York State earthquakes. Bulletin of the Seismological Society of America, 68(4), 1117-1131.

[6] **Boore, D. M., & Boatwright, J. (1984).** Average body-wave radiation coefficients. *Bulletin of the Seismological Society of America*, 74(5), 1615-1621.

[7] **Brune, J. N. (1971).** Correction to tectonic stress and the spectra of seismic shear waves from earthquakes. *J. Geophys. Res*, 76(20), 5002.

[8] **Brune, J.N. (1970).** Tectonic stress and the spectra of seismic shear waves from earthquakes. Journal of geophysical research 75 (26), 4997–5009.

[9] **Eshelby, J.D. (1957).** The determination of the elastic field of ellipsoidal inclusion, and related problems. Proceedings of the Royal Society of London A: pp. 376-396 1226.

[10] **Fehler, M. and Phillips, W.S. (1991).** Simultaneous inversion for Q and source parameters of microearthquakes accompanying hydraulic fracturing in granitic rock. Bull. Seismol. Soc. Am. 81 (2), 553–575.

[11] **Gibowicz, S.J., Young, R.P., Talebi, S. and Rawlence, D.J. (1991).** Source parameters of seismic events at the Underground Research Laboratory in Manitoba, Canada: scaling relations for events with moment magnitude smaller than 2. Bull. Seismol. Soc. Am. 81 (4), 1157–1182.

[12] **Goldstein, P. and Snoke, A. (2005).** SAC Availability for the IRIS Community. Incorporated Institutions for Seismology Data Management Center Electronic Newsletter, vol. II 1.

[13] **Haggag, H. M., Bhattacharya, P. M., Kamal, S. and Kayal, J. R. (2009).** Seismicity and 3D velocity structure in the Aswan Reservoir Lake area, Egypt. Tectonophysics, 476(3-4), 450-459.

[14] **Hanks, T. C. (1977).** Earthquake stress-dropsambient tectonic stresses, and stresses that drive plates. Pure Appl. Geophys. 115, 441 -458.

[15] **Hanks, T. C. and Kanamori, H. (1979).** A moment magnitude scale. Journal of Geophysical Research: Solid Earth, 84(B5), 2348-2350.

[16] **Hanks, T. C. and Wyss, M. (1972).** The use of body-wave spectra in the determination of seismic-source parameters. *Bulletin of the Seismological Society of America*, *62*(2), 561-589.

[17] **Kanamori, H. (1981).** The nature of seismicity patterns before large earthquakes.

[18] **Kanamori, H. and Brodsky, E. E. (2004).** The physics of earthquakes.Reports on Progress in Physics, 67(8), 1429.

[19] **Kanamori, H. (1977).** The energy released in great earthquakes. Journal of Geophysical.

[20] **Lay. T. and Wallac. T. C. (1995).** Modern global seismology. Elsevier.

[21] **Madariaga, R. (1976).** Dynamics of an expanding circular fault. Bull. Seismol. Soc. Am. 66 (3), 639–666.

[22] **Mandal, P., Rastogi, B.K. and Sarma, C.S.P. (1998).** Source parameters of Koyna earthquakes, India. Bull. Seismol. Soc. Am. 88 (3), 833–842.

[23] **Prochazkova, D. (1980).** Determination of source parameters. Publ. Ins. Geophys. Pol. Acad. Sci., A-9.135.

[24] **Saadalla, H, Abd el-aal, A.K., Abdelnasser M. and El-Faragawy., K. (2020).** A comprehensive study of the earthquake source, site, and path attenuation using body wave inversion in Aswan region, Egypt. NRIAG Journal of Astronomy and Geophysics. in press.

[25] **Saadalla, H., Mohamed, A., & El-Faragawy, K. (2019).** Determination of earthquake source parameters using the inversion of waveform data: A case of small earthquakes around High Dam Lake, Aswan region, Egypt. *Journal of African Earth Sciences*, *151*, 403-416.

[26] **Snoke, J. A. (2003).** FOCMEC: Focal mechanism determinations. *International Handbook of Earthquake and Engineering Seismology*, *85*, 1629-1630.

[27] **Zobin, V. M., Ivanova, E. I. and Chirkova, V. N. (1984).** Source parameters of earthquakes in Kamchatka and Commander Islands. Volcanol. Seismol, 2(6), 83-103.